JGR Solid Earth

RESEARCH ARTICLE
10.1029/2022JB024310

Special Section:
Understanding and anticipating Induced Seismicity: from mechanics to seismology

Competing Controls of Effective Stress Variation and Chloritization on Friction and Stability of Faults in Granite: Implications for Seismicity Triggered by Fluid Injection

Fengshou Zhang[1,2], Rui Huang[1,2], Mengke An[1,2], Ki-Bok Min[3], Derek Elsworth[4,5], Hannes Hofmann[6,7], and Xiaoguang Wang[8,9]

[1]Department of Geotechnical Engineering, College of Civil Engineering, Tongji University, Shanghai, China, [2]Key Laboratory of Geotechnical and Underground Engineering of Ministry of Education, Tongji University, Shanghai, China, [3]Department of Energy Resources Engineering and Research Institute of Energy and Resources, College of Engineering, Seoul National University, Seoul, Republic of Korea, [4]Department of Energy and Mineral Engineering, EMS Energy Institute and G3 Center, The Pennsylvania State University, University Park, PA, USA, [5]Department of Geosciences, The Pennsylvania State University, University Park, PA, USA, [6]Helmholtz Centre Potsdam GFZ-German Research Center for Geosciences, Potsdam, Germany, [7]Technische Universität Berlin, Berlin, Germany, [8]State Key Laboratory of Oil and Gas Reservoir Geology and Exploitation, Chengdu University of Technology, Chengdu, China, [9]Faculty of Land Resource Engineering, Kunming University of Science and Technology, Kunming, China

Abstract Fluids injection for hydraulic stimulation and fracturing, typical in the development of enhanced geothermal systems (EGS) in granites, can reactivate deep faults and induce seismicity. Such faults typically contain chlorite coatings as an alteration product that may impact styles of deformation—aseismic through seismic. We performed low velocity shear experiments on simulated granite fault gouges under conditions typifying a geothermal reservoir at ∼4-km depth with a confining pressure of 110 MPa, a temperature of 150°C, fluid pressures of 21–80 MPa, and chlorite contents of 0–100%, to investigate the influence of variation in effective stress and mineral composition on fault strength and stability. Our results show a transition from velocity-strengthening to velocity-weakening behavior in simulated granite gouge when the effective confining pressure was reduced from 89 to 30 MPa, characterized by a transition from fault compaction to dilation—as revealed by microstructural observations—with implications in enabling unstable failure. Conversely, increasing chlorite content stabilizes slip but reduces frictional strength. The microstructures of these mixed gouges exhibit shear localized on chlorite-enriched planes and promoting fault sliding. These results suggest that earthquake ruptures occurring during fluid injection can be facilitated by effective stress variations and that both controlling fluid overpressures (effective stresses) and being aware of the presence of alteration minerals are both important controls in mitigating such injection-induced seismic risks.

Plain Language Summary Enhanced geothermal systems (EGS) host an increasing number of induced earthquakes potentially linked to hydraulic stimulation. Rock cores recovered from geothermal reservoirs worldwide show an abundance of chlorite coatings on fault surfaces—present both natively and as a result of fluid circulation. To understand whether slip on deep fault will result in earthquakes, we measure the frictional properties of powdered granite fault rocks from the Pohang geothermal reservoir where an earthquake has occurred. We vary chlorite content and effective confining pressures and observe stable slip at higher effective confining pressures that transitions to unstable slip at lower effective confining pressures. Reducing the effective confining pressure destabilizes the fault behavior at in situ stress and temperature representative of the reservoir where an earthquake was observed. The addition of chlorite in the simulated gouge results in the opposite result, reducing the frictional strength but resulting in stable (aseismic) slip. Our results highlight the importance of effective stress variation and mineral composition in controlling fault frictional strength and stability, with their potential contributions to earthquake triggering.

Key Points:

- Effective stress variation and chloritization exert competing controls on friction and stability of granite faults
- Lower effective stress accentuates velocity-weakening behavior but retains high strength
- Conversely, chloritization reduces frictional strength but promotes stable failure

Supporting Information:

Supporting Information may be found in the online version of this article.

Correspondence to:

M. An,
2015mengkean@tongji.edu.cn

Citation:

Zhang, F., Huang, R., An, M., Min, K.-B., Elsworth, D., Hofmann, H., & Wang, X. (2022). Competing controls of effective stress variation and chloritization on friction and stability of faults in granite: Implications for seismicity triggered by fluid injection. *Journal of Geophysical Research: Solid Earth*, *127*, e2022JB024310. https://doi.org/10.1029/2022JB024310

Received 7 MAR 2022
Accepted 26 JUL 2022

Author Contributions:

Conceptualization: Rui Huang
Data curation: Mengke An
Investigation: Rui Huang
Methodology: Fengshou Zhang, Rui Huang
Resources: Ki-Bok Min
Supervision: Fengshou Zhang, Derek Elsworth
Validation: Fengshou Zhang, Mengke An
Writing – original draft: Rui Huang
Writing – review & editing: Fengshou Zhang, Mengke An, Ki-Bok Min, Derek Elsworth, Hannes Hofmann, Xiaoguang Wang

1. Introduction

High-pressure injection into the subsurface can reactivate critically stressed faults and trigger earthquakes. This phenomenon has been widely reported in numerous projects conducted in deep formation and has aroused public attention—including for enhanced geothermal systems (EGS), underground wastewater disposal and shale gas extraction (Bao & Eaton, 2016; Elsworth et al., 2016; Goebel & Brodsky, 2018; Grigoli et al., 2018; Kim

et al., 2018; Martínez-Garzón et al., 2014; Walsh & Zoback, 2015). For mature faults present close to such projects, the frictional properties of the fault gouge typically control fault rupture and seismic response (Ikari et al., 2011; Niemeijer & Collettini, 2014). Thus, detailed characterizations of the fault geometry and frictional properties are important in mitigating seismic risk for triggered earthquakes.

Hydraulic stimulation enhances the permeability of fractured reservoir through injection of high-pressure fluid. Fluid pressure in EGS reservoirs varies from a few MPa, to 89 MPa in the Pohang reservoir, or over 90 MPa in Espoo, Finland, respectively (Kwiatek et al., 2019; Park et al., 2020). Fluid overpressures, capable of reducing effective stresses and lowering fault strength, are one of the primary mechanisms that promote fault failure and trigger earthquakes. Prior studies have explored the role of dynamic fluid pressurization on fault frictional and stability properties, including pressurization due to fluid injections (e.g., Cappa et al., 2019; Larochelle et al., 2021; Passelègue et al., 2018; Sáez et al., 2022), thermal pressurization of fluids (e.g., Acosta et al., 2018; Badt et al., 2020; Brantut & Platt, 2017; Rice, 2006; Wibberley & Shimamoto, 2005), and mineral dehydration induced pressurization (e.g., Brantut et al., 2010; Hirose & Bystricky, 2007). However, limited laboratory studies focused on investigating the role of static fluid overpressure (i.e., effective stress variation) on fault frictional stability. Some show that increases in static fluid pressure result in a transition from stable to unstable frictional behavior (i.e., stick-slips), indicating that the static fluid overpressure is an important factor in promoting fault instability and further seismic slip (Sawai et al., 2016; Scuderi et al., 2017). Conversely, other experiments conducted on phyllosilicate-bearing gouges reveal that static fluid pressurization does not weaken the gouge—but instead promotes aseismic creep (An et al., 2020; de Barros et al., 2016; Scuderi & Collettini, 2018). This apparent contradiction in the impacts of static fluid pressurization on frictional stability implies a knowledge gap in our understanding of nucleation physics under static fluid overpressurization. Despite this contradiction, granites are typical EGS reservoir rocks, for which the effect of fluid overpressures or effective stress variations on frictional stability is poorly understood (Blanpied et al., 1998; Hong & Marone, 2005). Therefore, a systematic experimental study of slip instability in granites, specifically in response to static fluid overpressures, is needed to resolve the mitigating or reinforcing impacts of effective stress variations on instability.

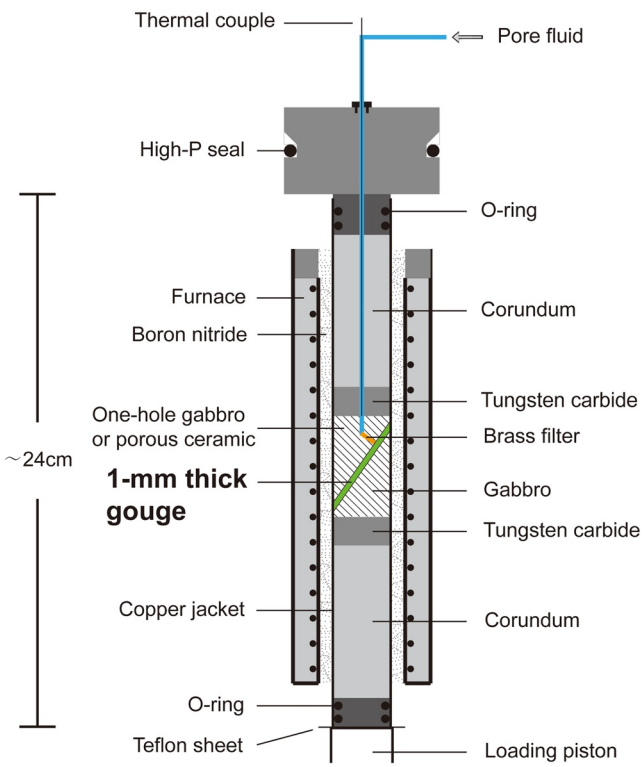

Figure 1. Schematic of the internal structure of the triaxial confining cell and testing apparatus.

Field investigations frequently document that chlorite is an important alteration mineral in greenschist facies and is a ubiquitous product of hydrothermal alteration (Elders et al., 1979; Schiffman & Fridleifsson, 1991). This is especially true within the fault cores within granites hosting geothermal reservoirs that are believed to play a significant role in modulating fault strength and stability (An et al., 2021; Kwon et al., 2019). Natural fractures in granite, recovered from borehole cores at 4.2-km depth from the Pohang geothermal reservoir, South Korea, show greenschist alteration along the fracture surface reaching 7 wt.% chlorite (An et al., 2021). Moreover, borehole cuttings (Well PX-2) at depths of 3,535–3,814 m show >10 wt.% chlorite with a maximum of 19 wt.% chlorite at a depth of 3,791 m (Lee et al., 2019). These observations are representative of other granites and confirm that chlorite can be a major component in geothermal reservoir rocks, and in controlling fault instability. To date, the effects of chlorite on frictional stability on faults in granite remains ambiguous, especially at high temperatures (Fagereng & Ikari, 2020; Okamoto et al., 2019).

Here, we specifically explore the impacts of effective stress variation on the frictional properties of simulated granite fault gouges containing chlorite to systematically evaluate the impacts of mineral composition and proportions. Experiments are conducted at stresses equivalent to a typical geothermal reservoir at a depth of ~4 km. These experiments are to: (a) determine the frictional properties of simulated granite and chlorite gouges under hydrothermal conditions; especially (b) the role of effective stress variation; (c) the role of chlorite content; and to then (d) use these observations to contextualize the response to reactivation in geothermal reservoirs.

Table 1
Experimental Matrix Defining Conditions and Key Data

Test ID	Gouge	σ_c (MPa)	P_f (MPa)	σ_{ceff} (MPa)	T (°C)	l_{final} (mm)	Observed response
Group1							
Gr-150-21	Pohang granite	110	21	89	150	3.44	vs
Gr-150-42	Pohang granite	110	42	68	150	2.96	vn
Gr-150-63	Pohang granite	110	63	47	150	3.59	vw
Gr-150-80	Pohang granite	110	80	30	150	3.29	vw
Group2							
Chl-150-42	Pure chlorite	110	42	68	150	3.74	vs
C1G9-150-42	Mixed (10% chlorite + 90% granite)	110	42	68	150	3.73	vs
C3G7-150-42	Mixed (30% chlorite + 70% granite)	110	42	68	150	3.66	vs
C5G5-150-42	Mixed (50% chlorite + 50% granite)	110	42	68	150	3.20	vs

Note. σ_c = confining pressure, P_f = fluid pressure, σ_{ceff} = effective confining pressure, T = temperature, l_{final} = final shear displacement, versus = velocity-strengthening, vn = velocity-neutral, vw = velocity-weakening.

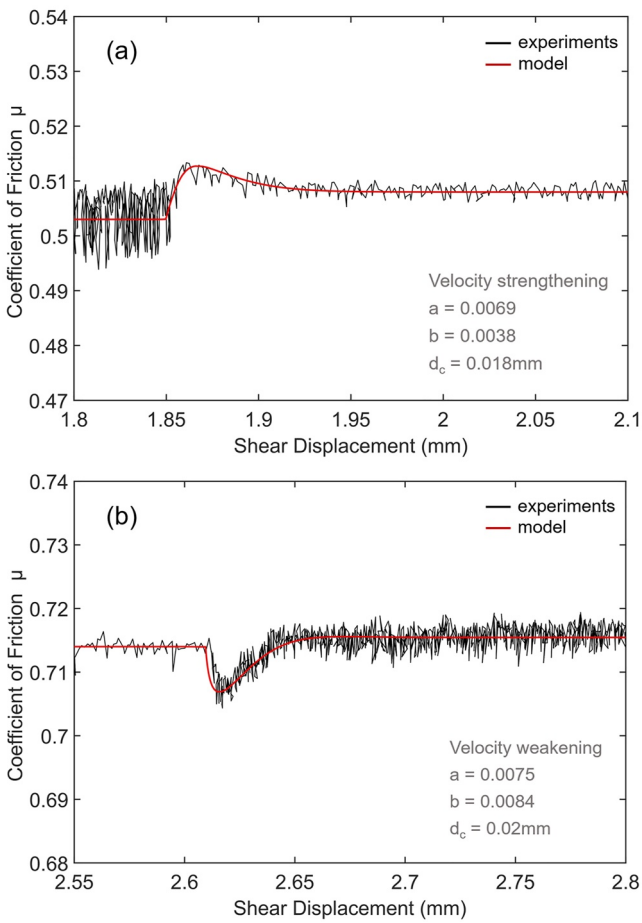

Figure 2. Typical fitting of data for (a) velocity-strengthening behavior in C5G5-150-42 (velocity-step of 0.244–1.22 μm/s) and (b) velocity-weakening behavior in Gr-150-63 (velocity-step of 1.22–0.244 μm/s).

2. Materials and Methods

2.1. Sample Preparation

We collected rock cores from ~4.2-km depth (Kwon et al., 2019) from the Pohang granodiorite. This is close (~300-m distance) to the hypocenter of the Mw 5.5 2017 fault reactivation, reflecting the frictional properties of the implicated fault. X-ray diffraction analysis (XRD) confirms the composition of the Pohang granite as 33% quartz, 47% albite, 8% microcline, 3% muscovite, and 9% chlorite by weight (Figure S1 in Supporting Information S1). The chlorite was collected from Fanshi County, Shanxi Province in northwest China and returns a >99% purity (Figure S2 in Supporting Information S1). To simulate the fault gouge, both the granite and chlorite samples were crushed and sieved to particles <75 μm.

2.2. Testing Procedure

Shear experiments were conducted in an argon gas-confined triaxial testing apparatus (Figure 1) located at the Institute of Geology, China Earthquake Administration, Beijing, China (He et al., 2006, 2007). The gouge sample is heated by a two-zone internal furnace with the fluid pressure elevated by a stepping-motor-driven pressure generator. An electro-hydraulic servocontrol system was used to drive the axial displacement. This apparatus can apply a confining pressure up to 420 MPa, a temperature up to 600°C, a fluid pressure up to 200 MPa, and an axial displacement rate down to 10^{-2} μm/s.

A 1-mm-thick layer of fault gouge inclined at 35° to the loading axis was sandwiched between gabbro driving blocks with dimensions of 20 mm in diameter and 40 mm in height. Two interconnected microboreholes in the upper driving block provide fluid access to the layer of fault gouge. To prevent extrusion of the fault gouge into this port and guarantee the low-pressure-loss transmission of fluid pressure, a brass filter caps the supply line at the edge of the fault gouge. The assembled sample was jacketed in a 0.35-mm-thick annealed copper sleeve. Double O-rings seal the sample against incursion of the argon gas into the gouge layer and are placed at both tips of the assembled sample. A thermocouple at the top of the apparatus monitors the changes in

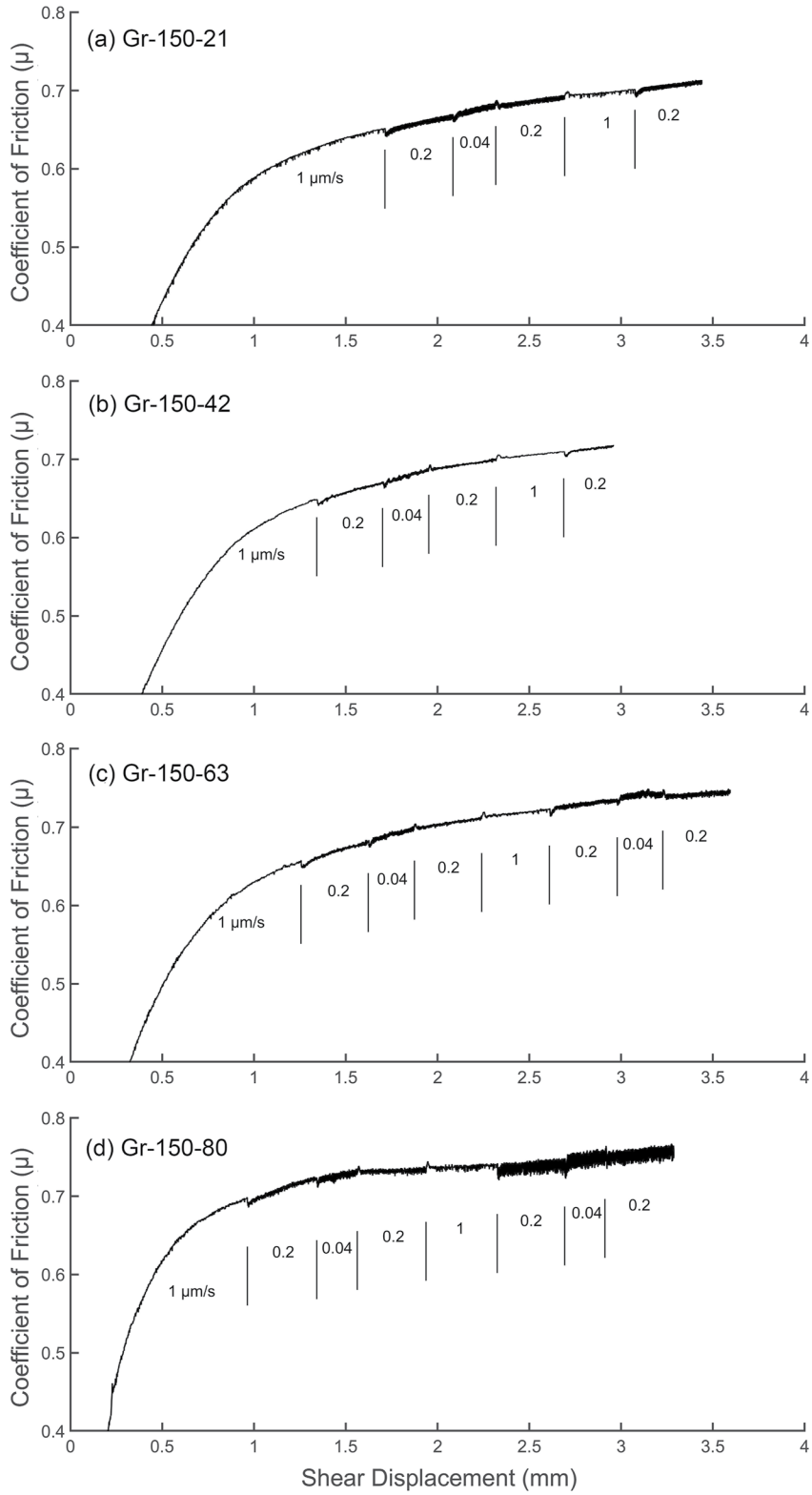

Figure 3. Friction-displacement curves for pure granite gouge at: (a) $P_f = 21$ MPa, $\sigma_{ceff} = 89$ MPa; (b) $P_f = 42$ MPa, $\sigma_{ceff} = 68$ MPa; (c) $P_f = 63$ MPa, $\sigma_{ceff} = 47$ MPa; (d) $P_f = 80$ MPa, $\sigma_{ceff} = 30$ MPa. The axial corresponding displacement rates (1–0.2–0.04 μm/s) are identified below the curves.

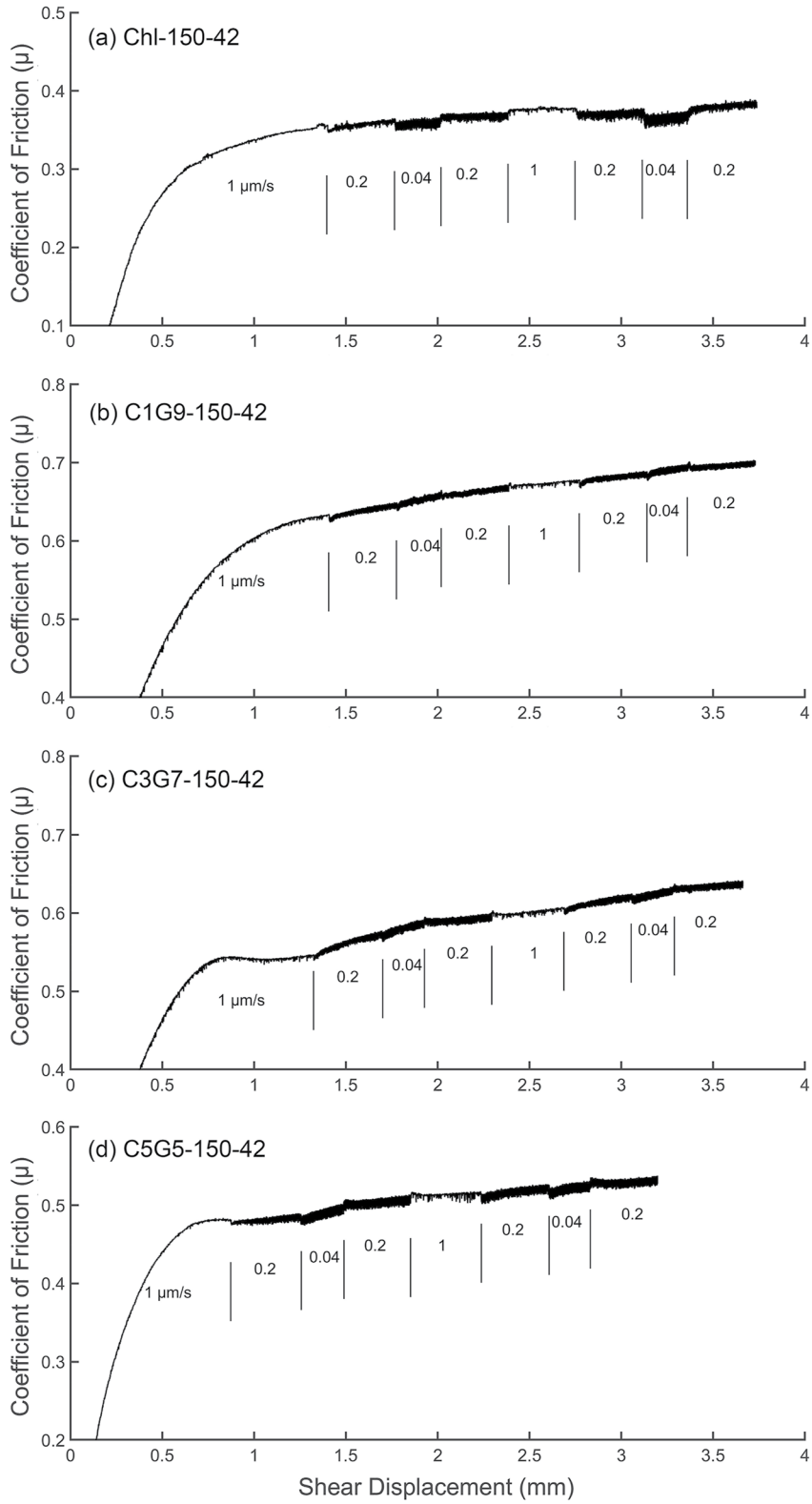

Figure 4. Friction-displacement curves for chlorite:granite mixtures at: (a) 100:0% (pure chlorite); (b) 10:90%; (c) 30:70%; and (d) 50:50%. The corresponding axial displacement rates (1–0.2–0.04 μm/s) are identified below the curves.

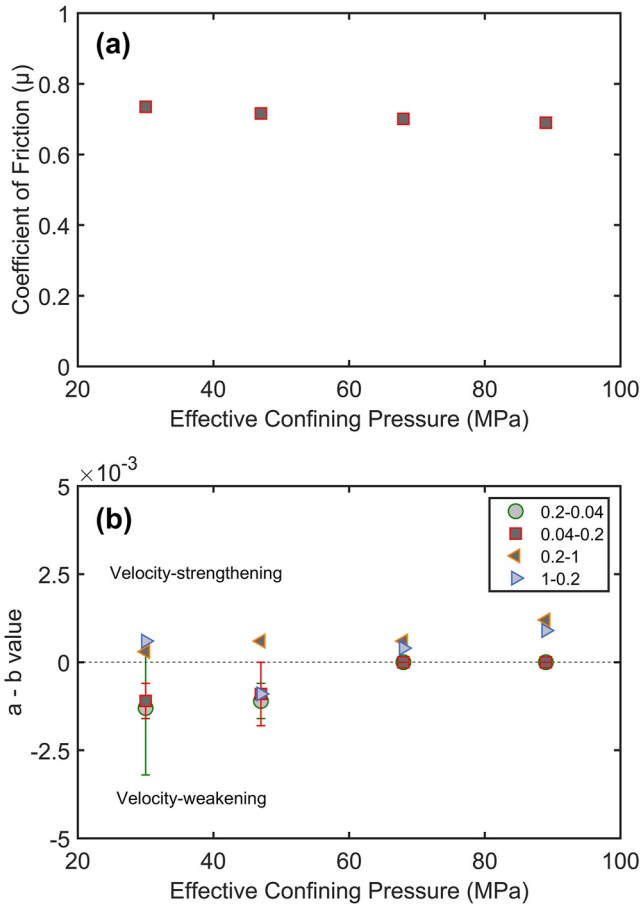

Figure 5. (a) Coefficient of friction μ and (b) frictional stability $(a-b)$ for the simulated granite gouge at varied effective confining pressures. The plotted values of $(a-b)$ are average values from the same velocity-steps in each experiment with the error bars representing the standard deviations. The legend shows the axial displacement rates.

temperature local to the fault gouge. The experiments typically begin by raising the gas confining pressure and axial load, then applying the fluid pressure and finally raising the temperature to desired values. Deionized water was adopted as the pore fluid to eliminate reactive chemical effects. When the pore fluid pressure was applied, the simulated gouge was saturated for >2 hr to ensure full saturation. In addition, to ensure that the chlorite gouge was fully saturated during the experiment, high permeability cylindrical porous ceramics were used as the upper driving blocks. All experimental data were recorded at a sampling frequency of 1 Hz.

We designed two groups of experiments based on the aims of the study. In Group 1, the fluid pressure was incremented from 21 to 80 MPa to investigate the impacts of effective stress variation on gouge friction and stability (Table 1). In Group 2, experiments on mixed granite/chlorite samples were performed to define the impacts of chlorite content on the frictional behavior of granite faults (Table 1). All experiments were conducted at a constant confining pressure (σ_c) of 110 MPa (corresponding to the lithostatic pressure at 4.2 km with a rock density of 2.630 g/cm^3) and a constant temperature (T) of 150°C (representing an in situ temperature at the 4.2-km depth of the Pohang geothermal reservoir). The constant fluid pressure (P_f) of 42 MPa set in Group 2 corresponds to the hydrostatic pressure at 4.2-km depth. The experiments involved shearing at an initial axial displacement rate of 1.0 μm/s with the axial displacement rates then stepped between 1.0, 0.2, and 0.04 μm/s at steady state (corresponding to 1.22, 0.244, and 0.0488 μm/s in the shear direction), to explore the velocity dependence of friction.

2.3. Data Analysis

To eliminate data errors ascribed to the decrease in contact area with shearing and the shear resistance from the copper jacket, the raw data were corrected following the methods described in He et al. (2006). The corrected data were then processed to obtain the corrected shear (τ) and normal stresses (σ_n). Frictional strength of the simulated fault gouge is defined by the friction coefficient μ as

$$\mu = \frac{\tau}{\sigma_{neff}} = \frac{\tau}{(\sigma_n - P_f)} \tag{1}$$

where the σ_{neff} is the effective normal stress.

The velocity dependence parameter $(a-b)$ was evaluated based on rate-friction and state-friction (RSF) theory (Dieterich, 1978, 1979; Marone, 1998; Ruina, 1983). In the framework of RSF theory, the coefficient of friction μ is expressed as

$$\mu = \mu_0 + aln\left(\frac{V}{V_0}\right) + bln\left(\frac{V_0\theta}{d_c}\right) \tag{2}$$

$$\frac{d\theta}{dt} = 1 - \frac{V\theta}{d_c} \tag{3}$$

where μ is the friction coefficient at the instantaneous shear velocity V, μ_0 is the friction coefficient at the reference shear velocity V_0, a and b are the friction parameters reflecting the direct and evolutionary effects of the shear velocity transition, respectively, with d_c denoting the critical slip distance over which frictional strength evolves to a new steady state, θ is a state variable that represents the renewal time of contact asperities. At a steady state of friction, the state variable θ is constant and thus $d\theta/dt = 0$ in Equation 3. Therefore, the velocity dependence parameter $(a-b)$ can be calculated based on Equations 2 and 3, expressed as

Table 2
Experimental Results for Coefficient of Friction (μ), Frictional Stability ($a-b$), and Frictional Constitutive Parameters a, b, and d_c

		$a-b$ ($\times10^{-3}$) at axial displacement rates (μm/s)				a ($\times10^{-3}$) at axial displacement rates (μm/s)				b ($\times10^{-3}$) at axial displacement rates (μm/s)				d_c (μm) at axial displacement rates (μm/s)			
Test ID	μ_{ss}	0.2–0.04	0.04–0.2	0.2–1	1-0.2	0.2–0.04	0.04–0.2	0.2–1	1-0.2	0.2–0.04	0.04–0.2	0.2–1	1-0.2	0.2–0.04	0.04–0.2	0.2–1	1-0.2
Gr-150-21	0.690	0	0	1.2	0.9	7.7	5.2	6.3	8.6	7.7	5.2	5.1	7.7	13	8	13	17
Gr-150-42	0.701	0	0	0.6	0.4	5.2	4.8	5.0	6.7	5.2	4.8	4.4	6.3	18	6	10	18
Gr-150-63	0.716	−1.1 ± 0.5	−0.9 ± 0.9	0.6	−0.9	5.2 ± 0.2	3.8 ± 0.7	5.4	7.5	6.3 ± 0.3	4.7 ± 0.2	4.8	8.4	18 ± 2	85 ± 5	11	20
Gr-150-80	0.735	−1.3 ± 1.9	−1.1 ± 0.5	0.3	0.6	11.1 ± 4.4	7.8 ± 2.3	7.9	15	12.4 ± 6.3	8.8 ± 2.7	7.6	14.4	17 ± 5	6 ± 1	8	15
Chl-150-42	0.368	4.7 ± 1.6	4.8 ± 0.5	4.6	4.3	9.4 ± 2	6.9 ± 0.3	5.7	8.6	4.7 ± 0.4	2.1 ± 0.3	1.1	4.3	18 ± 8	6 ± 1	5	8
C1G9-150-42	0.667	−0.3 ± 0.3	0	1.2	0.9	5.3 ± 0.8	5.6 ± 2.8	6.7	7.8	5.6 ± 1.1	5.6 ± 2.8	5.5	6.9	17	4 ± 1	5	20
C3G7-150-42	0.592	0.8 ± 1.4	1.5 ± 0.3	1.2	0.3	5.2 ± 0.2	4.3	7.5	5	3.8 ± 1	2.8 ± 0.3	6.3	4.7	21 ± 1	8	9	30
C5G5-150-42	0.504	2.2 ± 0.4	2.5 ± 1.3	3.1	2.5	6.5 ± 0.7	6.1 ± 0.3	6.9	9.3	4.4 ± 1.1	3.7 ± 1	3.8	6.8	18 ± 8	19 ± 9	20	42

Note. The coefficients of friction (μ) were determined at ~2.5 mm shear displacement and a shear velocity of 1.22 μm/s. The values of frictional stability ($a-b$) and frictional constitutive parameters a, b, and d_c are the average values from the same velocity-steps in each experiment and the errors represent the standard deviations. The first velocity-step (1.22-0.244 μm/s) was excluded in the calculation because it was not in the qualified steady state.

$$a-b=\frac{\mu-\mu_0}{\ln(V/V_0)}. \tag{4}$$

Faults with positive values of $(a-b)$ exhibiting velocity-strengthening behavior are intrinsically stable and promote aseismic slip. Conversely, negative values of $(a-b)$ indicate velocity-weakening behavior. Velocity-weakening behavior offers the potential for stick-slip and is a prerequisite for earthquake nucleation (Dieterich & Kilgore, 1996; Marone, 1998; Scholz, 1998).

We used an iterative least squares method to obtain the values of the constitutive parameters a, b, and d_c from the velocity-stepping experiments (Figure 2) (Blanpied et al., 1998; Reinen & Weeks, 1993). In addition, the constitutive laws of Equations 2 and 3 need to be incorporated with a description of elastic interaction between the fault gouge and the fault surroundings (Marone, 1998), expressed as

$$\frac{d\mu}{dt}=k(V_{lp}-V) \tag{5}$$

where k is the geometric stiffness of the fault in its surroundings (in this case the testing machine), V_{lp} is the velocity of load point and V is the true slip velocity.

At the conclusion of the experiments, we first used an oven to dry the deformed gouge samples at 75°C for 24 hr. Then, the dried samples were impregnated with low-viscosity epoxy under a vacuum. The thin sections were prepared by cutting the hardened samples perpendicular to the shear direction and along the sample axis when they were completely cured. Finally, all thin sections were polished and carbon coated for microstructural observation using the scanning electron microscopy (SEM).

3. Results

3.1. Impacts of Effective Stress Variation on Gouge Friction

Following the methods described in Section 2.2, shear experiments were conducted on the simulated granite, chlorite, or mixed gouges, with the friction-displacement curves presented in Figures 3 and 4. All experimental curves initially show a linear response, followed by yielding during an inelastic stage and finally followed by a slip hardening response. We measured the steady-state-friction coefficient at a shear offset of ~2.5 mm (corresponding to a shear velocity of 1.22 μm/s) for each experiment. A slip hardening response is observed for the granite-rich gouges (Figures 3, 4b, and 4c), but is less clearly apparent in the chlorite-rich gouges (Figures 4a and 4d). The slip hardening behavior is possibly due to an increase in contact area contributed by grain-size reduction through shear compaction (Scholz, 2002).

The coefficients of friction μ for the simulated granite gouge at varied effective confining pressures are in the range of 0.69–0.74 (Figure 5a and Table 2), consistent with previous work (Kilgore et al., 1993; Mitchell et al., 2016). The varied effective confining pressures result in a negligible increase in frictional strength (Figure 5a), implying that the variation in effective confining pressure exerts only a minor influence on the frictional strength. The velocity dependence of friction, recovered from velocity-stepping tests, is summarized in Figure 5b and Table 2. We find that the granite gouge exhibits an apparent transition from velocity-strengthening at $\sigma_{ceff}=89$ MPa ($a-b=0$ to 0.0012), to velocity-neutral at $\sigma_{ceff}=68$ MPa ($a-b=0$ to 0.0006), and then to velocity-weakening at $\sigma_{ceff}=47$ MPa ($a-b=-0.0018$ to 0.0006) through $\sigma_{ceff}=30$ MPa ($a-b=-0.0031$ to 0.0006) (Figure 5b). Similar

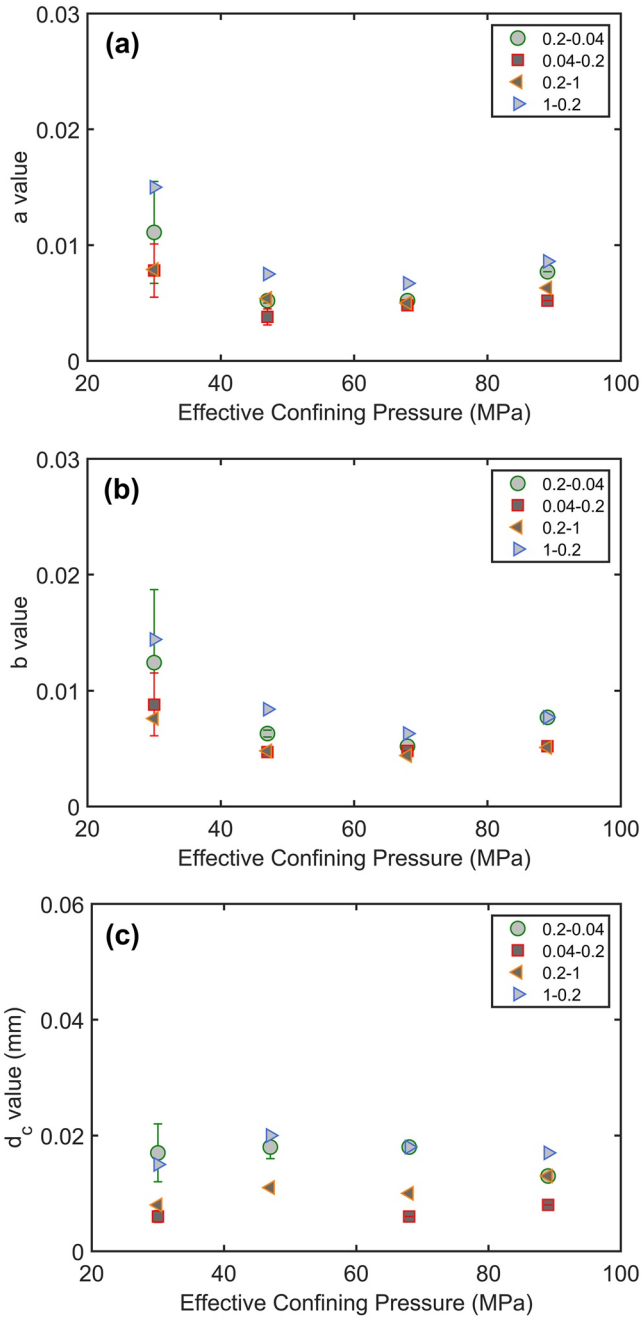

Figure 6. Friction constitutive parameters: (a) values of a, (b) values of b, and (c) values of d_c for the simulated granite gouge at varied effective confining pressures. The plotted frictional constitutive parameters a, b, and d_c are the average values from the same velocity-steps in each test with the error bars representing the standard deviations. The legends show the axial displacement rates.

results of fault instability prone to nucleate at lower effective stresses have been previously observed (e.g., He et al., 2007; Niemeijer & Collettini, 2014; Saffer & Marone, 2003; Sawai et al., 2016; Scuderi et al., 2017). In addition, from Figure 5b and Table 2, we observe that the $(a - b)$ values recovered between velocity upstepping and downstepping (e.g., 0.244–1.22 and 1.22-0.244 μm/s) may also be different. This discrepancy may arise from a more pronounced healing effect during velocity downstepping due to the lower post-shear velocity. Moreover, velocity upstepping promotes gouge dilation, while velocity downstepping promotes gouge compaction. This can also produce different $(a - b)$ values between the upstepped and downstepped velocities.

We further evaluate the response of friction constitutive parameters a, b, and d_c to variation in effective confining pressures. The parameters a and b both decrease with an increase in effective confining pressures (Figures 6a and 6b; Table 2). Our results are in accordance with other studies that observe that parameters a and b both decrease at higher effective stresses (Sawai et al., 2016). However, there is almost no variation in d_c across the range of our environmental conditions, indicating that d_c is little influenced by the effective confining pressures (Figure 6c and Table 2).

3.2. Effects of Chlorite Content on Gouge Friction

The pure chlorite gouge in our experiments is the weakest with $\mu = \sim 0.37$ (Figure 7a and Table 2), congruent with many previous studies (e.g., Moore & Lockner, 2004; Okamoto et al., 2019). Chlorite is a phyllosilicate mineral, but still stronger than other common phyllosilicates, such as illite ($\mu \sim 0.28$), talc ($\mu \sim 0.20$), or montmorillonite ($\mu \sim 0.13$) (Giorgetti et al., 2015; Tembe et al., 2010). The coefficient of friction μ decreases systematically with increasing chlorite content in granite/chlorite mixed gouges (Figure 7a and Table 2). Conversely, the velocity dependence of friction $(a - b)$ in granite/chlorite mixed gouges shows a monotonic increase with increasing chlorite content (Figure 7b and Table 2). Positive $(a - b)$ values paired with lower coefficients of friction μ are congruent with the relationship between the frictional strength and stability summarized by Ikari et al. (2011).

The variation in friction constitutive parameters a, b, and d_c of granite/chlorite mixed gouges for an increase in chlorite content are shown in Figure 8 and Table 2. Parameter a increases with increasing chlorite content, while parameter b conversely decreases (Figures 8a and 8b; Table 2). The responses of parameters a and b for increasing phyllosilicate content are significantly different in previous measurements (Giorgetti et al., 2015; Saffer & Marone, 2003), possibly due to the discrepancy in gouge materials and testing conditions. The characteristic length d_c increases monotonically with increasing chlorite content (Figure 8c and Table 2), congruent with previous observations (Fagereng & Ikari, 2020), but the pure chlorite gouge does not return a maximum magnitude of d_c in our measurements.

3.3. Microstructural Characterization

Microstructural observations reveal that the simulated granite gouges exhibiting velocity-strengthening behavior are distinct from those exhibiting velocity-weakening responses. At $\sigma_{ceff} = 89$ MPa (i.e., $P_f = 21$ MPa), the granite gouge shows velocity-strengthening behavior with the microstructure of the deformed gouge exhibiting particle crushing (Figure 9a). When the effective confining pressure is reduced to 68 MPa then 47 MPa, the granite gouges show velocity-neutral ($\sigma_{ceff} = 68$ MPa, $P_f = 42$ MPa) then velocity-weakening responses ($\sigma_{ceff} = 47$ MPa,

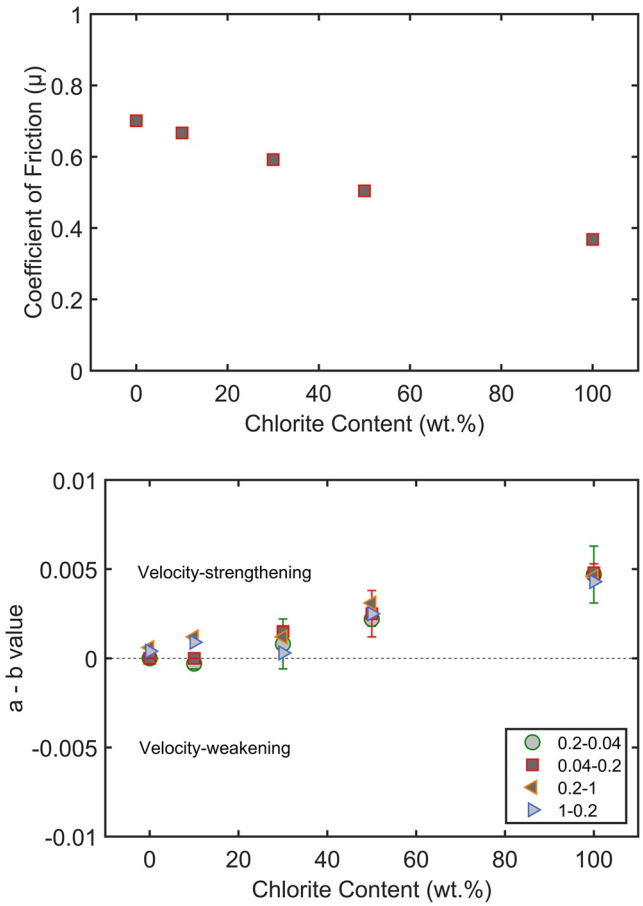

Figure 7. (a) Coefficient of friction μ and (b) frictional stability $(a - b)$ for granite/chlorite mixed gouges. The plotted values of $(a - b)$ are average values from the same velocity-steps in each experiment with the error bars representing the standard deviations. The legend shows the axial displacement rates.

P_f = 63 MPa). R_1-oriented and Y-oriented shears (Logan et al., 1992) develop together with an increase in variation of grain size as apparent in Figures 9b and 9c. The characteristic of a large variation of grain size is especially evident in the deformed granite gouge that sheared at σ_{ceff} = 30 MPa (i.e., P_f = 80 MPa) and exhibits the strongest velocity-weakening behavior (Figure 9d).

In contrast to the granite gouges, the granite/chlorite mixed gouges all exhibit velocity-strengthening behaviors. In addition, less obvious localized shear zones and foliation enrichment are found in these chlorite-rich gouges (Figures 10a and 10b). Well-developed foliations aligned with the shear direction are observed in pure chlorite gouge, and shear is distributed homogeneously throughout the gouge (Figure 10a). In the 50:50 chlorite:granite gouge, chlorite foliations wrap around the granite gouge particles, and deformation is mainly concentrated in chlorite-rich shear zones (Figure 10b). In summary, the microstructure of deformed velocity-strengthening gouge is characterized by particle crushing or elongation with the development of a finer and more uniform grain size (Figures 9a, 10a and 10b), whereas velocity-weakening response promotes localized shear characterized by a large variation in grain size (Figures 9b–9d).

4. Discussion

4.1. Mechanistic Impact of Effective Stress Variation on Fault Stability

The shear experiments with granite gouges conducted at varied effective confining stresses define two regimes of velocity dependence—these are velocity-strengthening response $(a - b > 0)$ at σ_{ceff} = 68–89 MPa and velocity-weakening response $(a - b < 0)$ at σ_{ceff} = 30–47 MPa (Figure 5b). Sawai et al. (2016) conducted friction experiments on blueschist powder at effective normal stresses of 0–200 MPa and temperatures of 22–400°C. They reported that a transition from velocity-strengthening to velocity-weakening occurred when decreasing effective normal stress to ~70 MPa at temperatures of 100–300°C. Such a similar velocity-weakening response has also been presented for phyllosilicate-bearing fault rocks with decreasing effective normal/confining stresses (Niemeijer & Collettini, 2014). From these results, the effective normal/confining stress is apparently important in controlling the transition from velocity-strengthening to velocity-weakening behavior. Meanwhile, the responses of fault stability also depend on the mineral composition, temperature, and sliding velocity.

The changes in velocity dependence $(a - b)$ with effective normal/confining stress can be partially explained by a microphysical model involving shear-rate dependent modes of mass transfer (den Hartog & Spiers, 2013, 2014; Niemeijer & Spiers, 2007). In this model, friction is potentially modulated by a competition between shear-induced dilation, associated with granular flow, transitioning to thermally activated compaction modulated by pressure solution. A lower effective normal/confining stress will decrease rates of mass transfer by pressure solution (Yasuhara & Elsworth, 2004), and thus yield a decrease in the relative importance of thermally activated compaction, relative to shear-induced dilation. In this process, the shear deformation can no longer be accommodated by compaction through pressure solution and the gouge must therefore dilate to accommodate slip—resulting in an elevated steady-state porosity. This in turn indicates a decrease in intergranular contact area at steady state due to the higher porosity. As a consequence, the steady-state-frictional strength is reduced, the parameter b is increased, and the velocity dependence $(a - b)$ is reduced—contributing to the observed velocity-weakening behavior.

Our results indeed show that the parameter b increases with decreasing effective confining stress (Figure 6b), suggesting a contact area decrease or porosity increase under lower effective confining stress conditions. Although we do not directly measure the gouge porosity, the microscopic observations provide a reasonable proxy. The

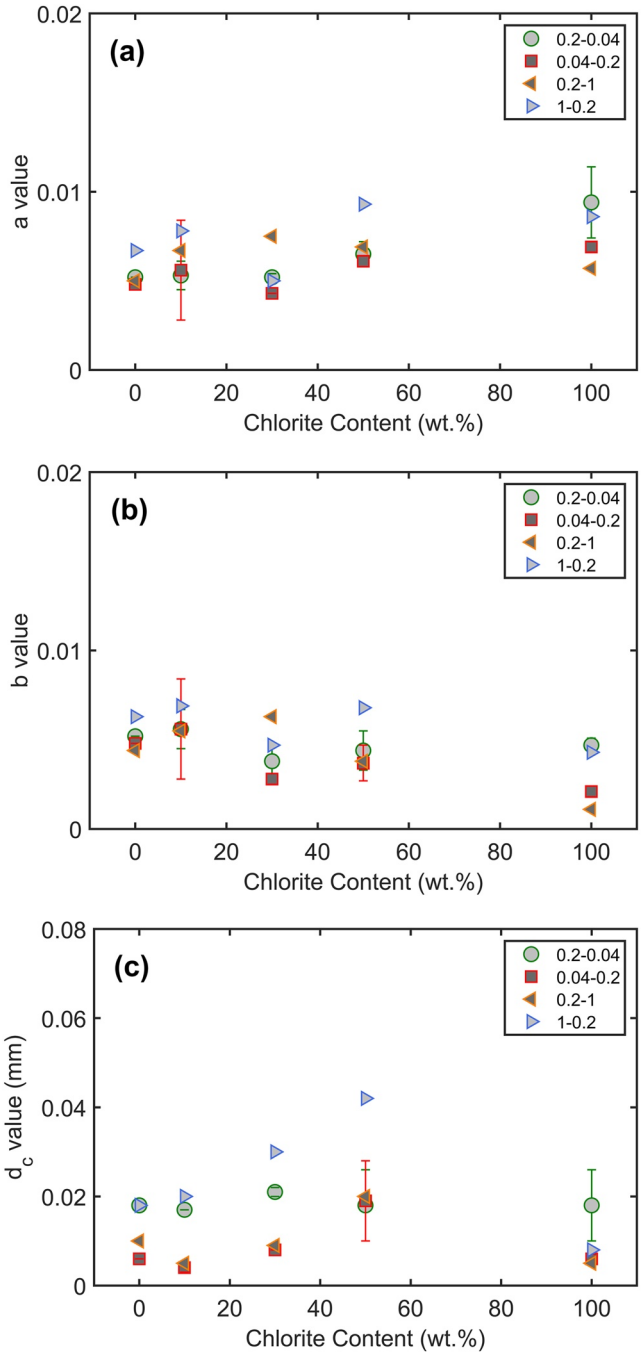

Figure 8. Friction constitutive parameters: (a) values of a, (b) values of b, and (c) values of d_c for granite/chlorite mixed gouges. The plotted frictional constitutive parameters a, b, and d_c are the average values from the same velocity-steps in each test with the errors representing the standard deviations. The legends show the axial displacement rates.

microstructures of the granite gouges deformed at higher effective confining stresses exhibit a dense structure—a lower porosity, characterized by a compaction-dominated response, and corresponding to velocity-strengthening (Figures 11a and 11b). Conversely, the gouges at lower effective confining stresses form a discrete structure—a higher porosity characterized by a dilation-dominated response corresponding to velocity-weakening behavior (Figures 11c and 11d). An elevated porosity resulting in velocity-weakening behavior has also been documented in other laboratory studies on granite fractures (Ishibashi et al., 2018). This is also congruent with field observations that faults tend to dilate during seismic slip (Guglielmi et al., 2015). The transition from net compaction to dilation with decreasing effective confining stress indicates that a lower effective confining stress can reduce cataclasis and its impact on grain-size reduction by weakening the effect of compaction and thus accentuating fault dilation, contributing to an elevated porosity, and thereby changing the velocity dependence of friction. This observation is consistent with the results of Acosta et al. (2020, 2022) in terms of the permeability evolution of calcite bearing faults. The fault shear induces dilatancy at low effective stress but contributes to more compaction at high effective stress. The general concept of competition between compaction and dilation is useful in interpreting our observations of changes in the velocity dependence of friction as a function of effective confining stress and velocity. Our results emphasize the importance of variations in effective confining stress as a key factor in controlling fault instability in terms of a competition between compaction and dilation.

In addition, we observe that the friction coefficient is insensitive to variations in effective confining stresses, whereas the velocity dependence is highly sensitive (Figure 5). These observations further demonstrate that the variation in effective confining stress imparts an intrinsically time-dependent response which is expected to affect, and to be affected-by, the dissolution and reaction of minerals—thereby contributing to a pronounced impact on velocity dependence of friction. A more evident change in velocity dependence of $(a - b)$ with decreasing effective stress at relatively low slip velocity also supports this idea (Figure 5b).

4.2. Evolution of Friction With Elevated Chlorite Content

We observe that homogeneously mixed gouges of granite/chlorite exhibit almost pure velocity-strengthening behaviors when >30 wt.% chlorite (at hydrothermal conditions representative of a reservoir at ~4-km depth (Figure 7b)) contrary to the pure granite gouge exhibiting velocity-neutral behavior. We extrapolate this to imply that the presence of chlorite within the principal slip zone (PSZ) of a fault will promote aseismic slip and fault creep. Our results show that the friction coefficient decreases monotonically with increasing chlorite content in mixed granite/chlorite gouges (Figure 7a), signifying that the participation of chlorite may at the same time weaken but stabilize such faults.

The persistent weakness of a fault with increasing chlorite content, in our experiments, indicates a potential change in deformation mechanism for slip behavior. To investigate the role of chlorite in inducing fault weakness, we compare the deformed characteristic microstructures between the 100% granite and the 50:50 chlorite:granite gouges. Cataclastic flow is clearly evident in microstructures with some fine grains surrounding the relatively larger grains in the 100% granite gouge (Figure 12a). This phenomenon can be attributed to comminution occur-

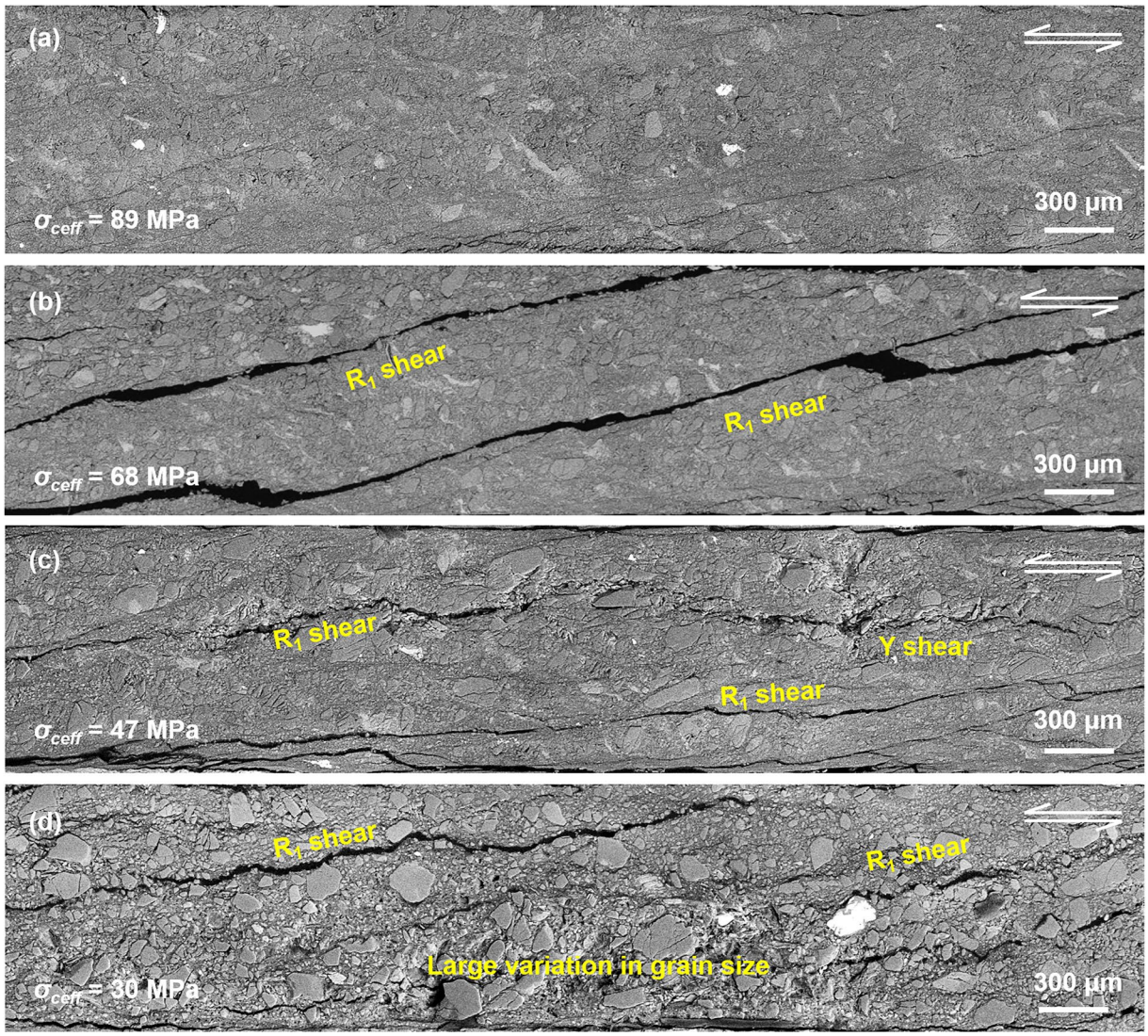

Figure 9. Microstructures (backscattered images) of the deformed granite gouges for shear experiments at (a) $\sigma_{ceff} = 89$ MPa, (b) $\sigma_{ceff} = 68$ MPa, (c) $\sigma_{ceff} = 47$ MPa, and (d) $\sigma_{ceff} = 30$ MPa.

ring at contacting asperities between large grains through a process of cataclastic flow, suggestive of plastic deformation at grain-to-grain contacts which favor velocity-weakening (Baumberger & Caroli, 2006; Dieterich & Kilgore, 1994; Fagereng & Ikari, 2020; Ikari et al., 2016). The R_1 shear exhibited in 50:50 chlorite:granite mixed gouge is more continuous than that in the 100% granite gouge and is characterized by enrichment of chlorite foliation with very small grains enhanced in zones of high concentration of shear strain (Figure 12b; Giorgetti et al., 2015). The development of a network of chlorite foliations surrounded by fine grains establishes a localized shear zone (Figure 12b), implying that the deformation mechanism evolves from distributed cataclastic flow (100% granite gouge) to localized frictional sliding along chlorite-rich R_1 shears (50:50 chlorite:granite gouge), thus resulting in a decrease in frictional strength. This mechanism of shear strain accommodated by phyllosilicate foliation is equivalent to the fault becoming persistently weak once the phyllosilicate-rich network matures and then dominates the mode of frictional sliding (Collettini et al., 2009; Okamoto et al., 2019). The occurrence of shear that localizes on chlorite-enriched planes is one suitable mechanism to explain the weakening with increasing chlorite content.

We observe that the frictional parameter b is near-zero for all chlorite contents (Figure 8b). In terms of RSF theory, the physical significance of the parameter b is in describing the evolution of contact area over a critical

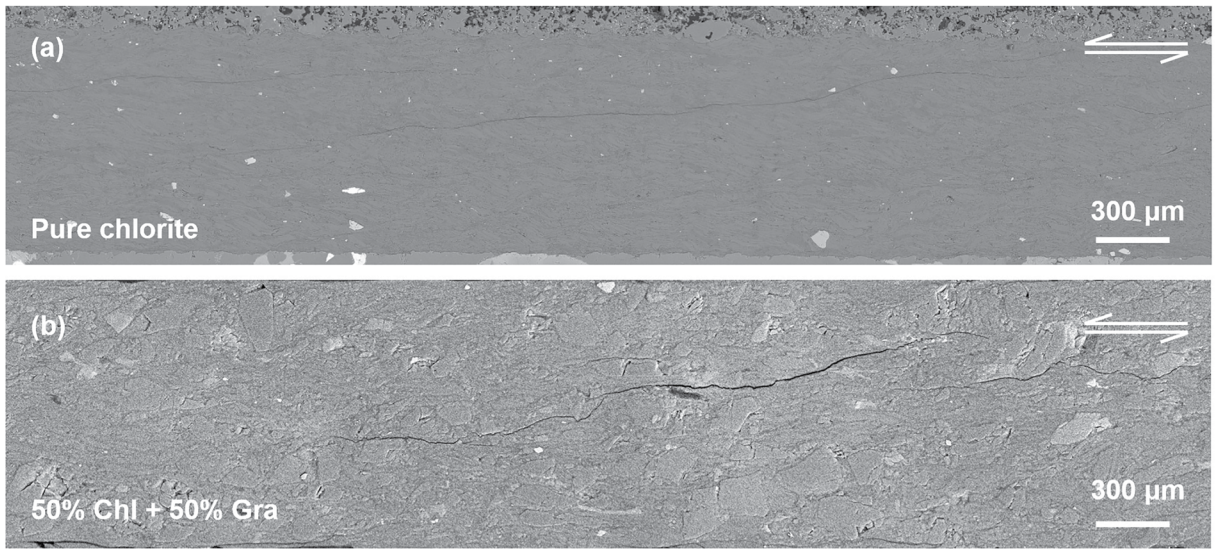

Figure 10. Microstructures (backscattered images) of the deformed (a) pure chlorite gouge and (b) 50:50 chlorite:granite gouge after shear experiments.

slip distance d_c (Scholz, 1998). Our microstructural observations for pure chlorite show that the alignment of the elongated chlorite particles results in a layered structure (Figure 13a). We infer that this layered structure favors maximizing the contact area and minimizing the evolution of contact area when changing the slip velocity, and thus driving b to approach zero. Our observations are consistent with the phenomenon of "contact saturation" (Saffer & Marone, 2003; see also Ikari et al., 2009). Thus, a near-zero value for b, also observed in pure smectite gouge, results in the assumption that the clay particles are in complete contact with no further potential for the contact area to evolve/increase. Our microstructural observations on pure chlorite gouge represent a documentable demonstration of this effect (Figure 13b). This might also be the reason why slip hardening is less developed in chlorite-rich gouges (Figures 4a and 4d). Since the particles are already in "complete" contact, due to a high proportion of chlorite, the frictional strength would no longer change with continued sliding. Our data suggest that the "contact saturation" effect, arising from clay grain alignment, is a key factor in modulating the velocity dependence of friction in clay-rich gouges.

4.3. The Role of Chlorite in EGS Development

Chlorite is a common rock-forming mineral that forms readily at both low and high temperatures (Browne, 1978). Present not only in the Pohang geothermal reservoir, numerous geothermal reservoirs worldwide document the presence of chlorite as a hydrothermal alteration product. This presence is documented over the broad temperature range 80–380°C but is more frequently apparent within the range 150–250°C (Arnórsson, 1995; Cathelineau & Nieva, 1985; Cavarretta et al., 1982; Elders et al., 1979; Gebregzabher, 1986; Reyes, 1990; Seki et al., 1983; Steiner, 1968). These temperature ranges correspond to typical temperature gradients in the range 30–50°C/km and representative of a depth of 4–5 km—common to many EGS reservoirs (Olasolo et al., 2016). The Pohang granite samples recovered from 4.2 km display a native presence of 9 wt.% chlorite, with borehole cuttings (3,535–3,814-m depth) returning a maximum of 19 wt.% chlorite. In addition, granite cores obtained from the Gonghe geothermal system in Qinghai, China, show chlorite enrichment (2,900–3,500-m depth) reaching to 34 wt.% chlorite at 3,500-m depth (Table 3) (Figures S3–S6 in Supporting Information S1). These field data therefore suggest that chlorite may exert a strong control on the frictional properties of granitic EGS reservoir rocks due to its high relative abundance.

As noted by Elders et al. (1979), the pattern of heat transfer and fluid flow determines the distribution of hydrothermal mineral assemblages. Thus, the high temperatures and induced fluid circulation characteristics of geothermal reservoirs could facilitate the transition of typical shallow-habit phyllosilicate minerals, such as montmorillonite or kaolinite, into illite plus chlorite—resulting in a typical clay-mineral assemblage formed at higher temperature (e.g., >145°C; Browne, 1978). This may be the cause of enrichment of chlorite as a temperature-dependent

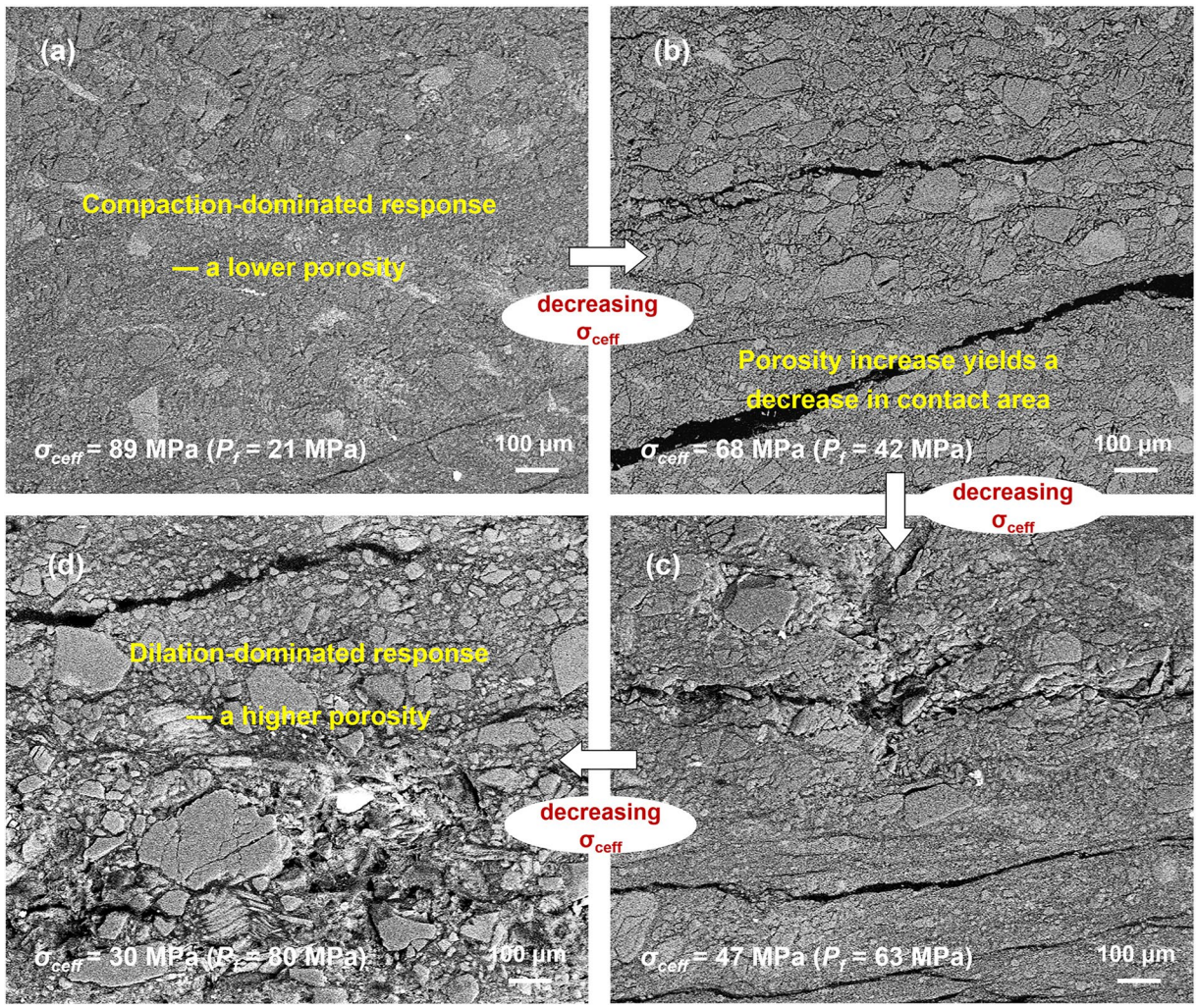

Figure 11. A transition from compaction-dominated to dilation-dominated shear response with decreasing effective confining stress observed in granite gouges: (a) σ_{ceff} = 89 MPa, (b) σ_{ceff} = 68 MPa, (c) σ_{ceff} = 47 MPa, and (d) σ_{ceff} = 30 MPa.

mineral in geothermal reservoirs. Our results reveal that chlorite is frictionally weak and capable of promoting fault slip but of maintaining stable sliding. This effect can be more profound if the fault zone is highly permeable, favoring invasion by hydrothermal fluids, and facilitating alteration by metasomatism on the fault surface. This, in turn, would result in increased chloritization of the fault surface to significantly weaken the fault but induce stable fault sliding. Therefore, the chlorite content should be determined in geothermal sites to evaluate the fault reactivation potential and fault slip mode triggered by fluid injection.

4.4. Implications for Induced and Natural Seismicity

Our results have important implications for the generation of induced seismicity in deep geothermal reservoirs and wastewater disposal projects, both proximal to basement rocks, and also offers insights into natural seismicity in other environments. EGS and wastewater disposal each involve the injection of large volumes of water into deep formations, significantly increasing fluid pressures and reducing effective stresses. Many EGSs reach to 4–5 km, and temperatures are typically over 150°C. Forced fluid injection reduced the effective stresses to <30 MPa at 4,200-m depth at the Pohang EGS site (e.g., in situ effective normal stresses of σ_{Hmax} = 153.8 MPa, σ_{hmin} = 30.8 MPa, and σ_v = 16.8 MPa reduced by a maximum overpressure of 89.2 MPa during hydraulic stimulation of well PX-2, Lee et al., 2019), with our results (without chlorite) suggesting that any fault reactivation will likely be velocity-weakening—to potentially produce unstable sliding and trigger earthquakes. Dehydration reac-

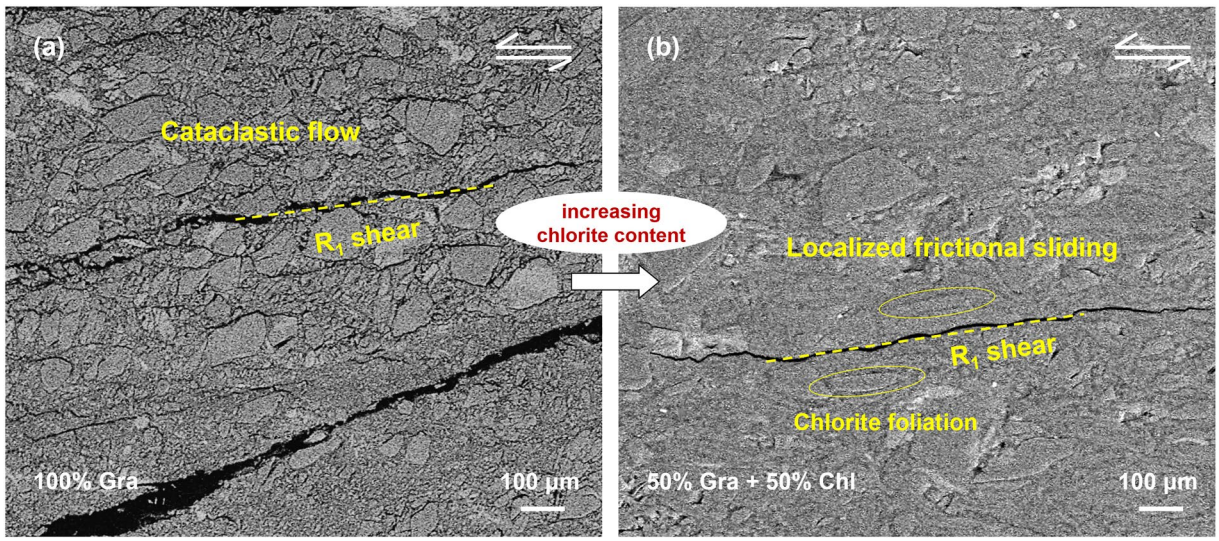

Figure 12. A comparison of microstructure deformation characteristics between the (a) 100% granite and (b) 50:50 chlorite:granite gouges, indicating a potential change of deformation mechanism.

tions may also release water from hydrous minerals through metamorphism, suggested as an important control on fault instability for megathrust earthquakes in subduction zones (Brantut et al., 2010; Chapman et al., 2022; Davis et al., 1983; Hirose & Bystricky, 2007; Sawai et al., 2016) and may add to this effect—although the "openness" of the system is likely to make this a small secondary effect. For faults containing mixed gouges of granite and chlorite, a low chlorite content can reduce fault frictional strength and promote fault failure but under stable sliding. The localized frictional behavior observed in chlorite-rich gouge provides insight that, if chlorite is abundant in natural faults, slip could localize along a weak layer since the chlorite is energetically prone to deform. From our experimental results of Figures 5 and 7, decreasing the effective confining pressure from 89 to 30 MPa decreases $(a - b)$ values of ~2.5e−3, while increasing the chlorite content from 0 to 50 wt.% increases $(a - b)$ values also around 2.5e−3. This implies that the impact of chlorite may compensate for the impact of stress, with regard to controls on frictional stability. However, the chlorite content in the Pohang geothermal reservoir (South Korea) is generally below 20 wt.% (Lee et al., 2019) and the highest chlorite content in the Gonghe geothermal reservoir approaches 35 wt.% (Table 3), all much lower than the 50 wt.% content. This suggests that a low chlorite content may not totally compensate for the stress effect for frictional stability. Our results hence imply fault

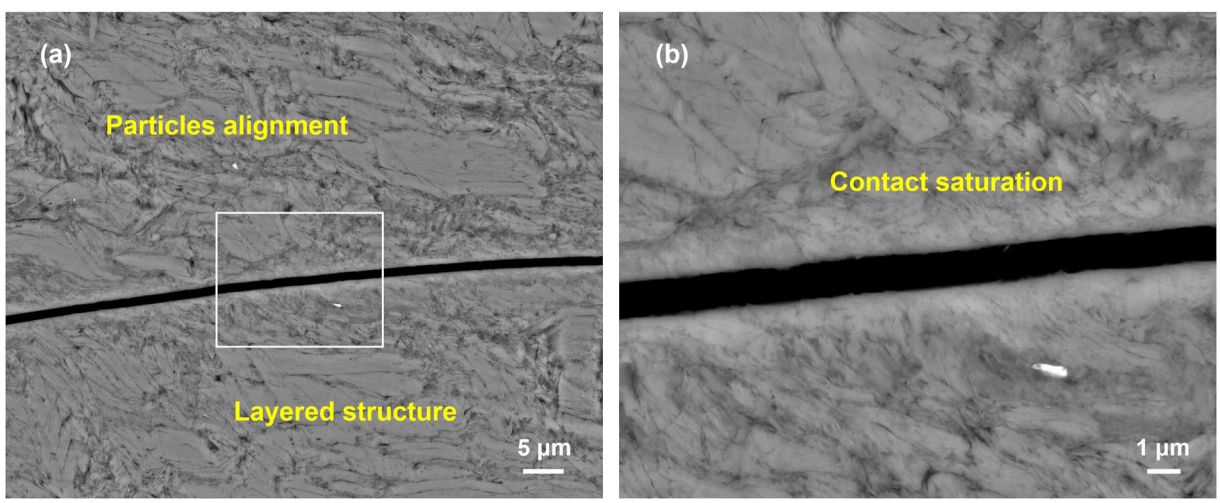

Figure 13. Microscopic observations for the deformed pure chlorite gouge. Panel (b) represents a zoom-in of the white outline in (a).

Table 3
Mineral Compositions in Granite Cores From Well GR-1 in the Gonghe Geothermal Reservoir, Qinghai, China

Depth (m)	Quartz	Plagioclase	Chlorite	Microcline	Calcite	Mica	Laumontite
2,900	43	20	**20**	12	3	2	0
3,250	56	9	**18**	1	10	7	0
3,400	49	28	**14**	4	0	3	2
3,500	27	14	**34**	10	8	4	3

Note. Measured by XRD (wt.%). The bold values highlight the abundance of chlorite in Gonghe Geothermal Reservior.

slip is promoted by the weakening presence of chlorite but fault instability is conversely promoted by reduced effective pressures—defining basic first-order controls on fault strength and stability and suggesting the potential for control.

In addition, our results on the influence of effective stress variation have important implications for understanding the relation between fault stability and permeability. The hydraulic transport properties of calcite bearing faults are impacted by surface geometry and applied stresses for rough fractures or faults (Acosta et al., 2020, 2022). Reducing the effective stress will promote fault dilatancy and generate large permeability increases. Combined with our results, the instability of a granite fault at lower effective stresses may be accompanied by an increase in reservoir permeability during EGS development. Our effective pressure-induced transition of frictional stability to instability on granite fault gouge is also similar to the reported brittle-ductile transition (BDT) in porous rocks (Baud et al., 2021; Wong & Baud, 2012). At lower effective confining stresses, brittle faulting is generally observed with dilatant deformation accompanied by shear localization. Conversely, shear-enhanced compaction may be developed with this leading to either delocalized cataclastic flow or compaction band deformation. Our observed microstructures (Figure 11) confirmed similar mechanisms of a pressure-induced stability-instability transition with the BDT, indicating that the mechanisms of BDT in porous rocks can also explain the stability-instability transition in porous fault gouge. Both transitions are important in understanding the deformation during faulting and in earthquake rupture.

5. Conclusions

We measured friction and stability on simulated samples of Pohang granite gouges and on fabricated mixed gouges of granite/chlorite under hydrothermal conditions, to separately investigate the impacts of effective stress variation and mineral composition. These laboratory observations result in the following conclusions:

1. A transition from velocity-strengthening to velocity-weakening response is observed with decreasing effective confining pressures in the simulated granite gouge sheared under hydrothermal conditions. This indicates that the reduction in effective stresses promote frictional instability by controlling the competition between fault compaction and dilation.
2. Chlorite-rich gouges return much lower frictional strengths than granite gouge. Shear is observed to localize on chlorite-enriched planes. This localized slip is suggested as a mechanism to explain the increase in fault weakness with increasing chlorite content. In addition, the parameter b, responsible for the evolution of friction, decreases to near-zero with increasing chlorite content, suggesting that "contact saturation" in clay-rich gouges is a viable mechanism in controlling the velocity dependence of friction.
3. Since fault instability caused by injection typically results from elevated pore fluid pressure and related reduction in effective frictional strength, we infer that earthquake ruptures triggered during fluid injection can also be facilitated by effective stress variations. Concurrently, faults containing chlorite-rich gouges may be readily reactivated. Thus, the effective stress variations and the presence of alteration minerals should jointly be taken into account to mitigate injection-induced seismic risks.

Data Availability Statement

The friction data in this work can be found at https://doi.org/10.5061/dryad.tb2rbp02j.

Acknowledgments
This research was funded by the National Natural Science Foundation of China (42077247, 42107163), the China Postdoctoral Science Foundation (2021M692448, 2022T150483), and the Fundamental Research Funds for the Central Universities. The recovery of rock core from the Pohang EGS site was initially sponsored by a Grant (No. 20123010110010) from the New and Renewable Energy Program of the Korea Institute of Energy Technology Evaluation and Planning, and funded by the Ministry of Trade, Industry and Energy of the Korean Government. KM was supported by the Innovative Technology Development Program for High-level waste management of the National Research Foundation of Korea (NRF) funded by the Korea government (Ministry of Science and ICT, MSIT) (Grant No. 2021M2E3A2044264). DE acknowledges the support from G. Albert Shoemaker endowment. HH is grateful for the support by the Helmholtz Association's Initiative and Networking Fund for the Helmholtz Young Investigator Group ARES (Contract No. VH-NG-1516). We appreciate the assistance of Jianye Chen and Wenming Yao in conducting the experiments. We thank the helpful reviews from Joel Sarout and Mateo Acosta.

References

Acosta, M., Maye, R., & Violay, M. (2020). Hydraulic transport through calcite bearing faults with customized roughness: Effects of normal and shear loading. *Journal of Geophysical Research: Solid Earth*, *125*, e2020JB019767. https://doi.org/10.1029/2020JB019767

Acosta, M., Maye, R., & Violay, M. (2022). Hydraulic transport properties of calcite bearing faults with customized roughness: Revisiting hydro-shear stimulation techniques. In *Proceedings of the 47th Workshop on Geothermal Reservoir Engineering*. Stanford, CA: Stanford University. SGP-TR-223. Retrieved from https://pangea.stanford.edu/ERE/db/GeoConf/papers/SGW/2022/Acosta.pdf

Acosta, M., Passelègue, F. X., Schubnel, A., & Violay, M. (2018). Dynamic weakening during earthquakes controlled by fluid thermodynamics. *Nature Communications*, *9*(1), 3074. https://doi.org/10.1038/s41467-018-05603-9

An, M., Zhang, F., Chen, Z., Elsworth, D., & Zhang, L. (2020). Temperature and fluid pressurization effects on frictional stability of shale faults reactivated by hydraulic fracturing in the Changning block, southwest China. *Journal of Geophysical Research: Solid Earth*, *125*, e2020JB019584. https://doi.org/10.1029/2020JB019584

An, M., Zhang, F., Min, K., Elsworth, D., Marone, C., & He, C. (2021). The potential for low-grade metamorphism to facilitate fault instability in a geothermal reservoir. *Geophysical Research Letters*, *48*, e2021GL093552. https://doi.org/10.1029/2021GL093552

Arnórsson, S. (1995). Geothermal systems in Iceland; structure and conceptual models; I. High-temperature areas. *Geothermics*, *24*(5–6), 561–602. https://doi.org/10.1016/0375-6505(95)00025-9

Badt, N. Z., Tullis, T. E., Hirth, G., & Goldsby, D. L. (2020). Thermal pressurization weakening in laboratory experiments. *Journal of Geophysical Research: Solid Earth*, *125*, e2019JB018872. https://doi.org/10.1029/2019JB018872

Bao, X., & Eaton, D. W. (2016). Fault activation by hydraulic fracturing in western Canada. *Science*, *354*(6318), 1406–1409. https://doi.org/10.1126/science.aag2583

Baud, P., Hall, S., Heap, M. J., Ji, Y., & Wong, T.-F. (2021). The brittle-ductile transition in porous limestone: Failure mode, constitutive modeling of inelastic deformation and strain localization. *Journal of Geophysical Research: Solid Earth*, *126*, e2020JB021602. https://doi.org/10.1029/2020JB021602

Baumberger, T., & Caroli, C. (2006). Solid friction from stick-slip down to pinning and aging. *Advances in Physics*, *55*(3–4), 279–348. https://doi.org/10.1080/00018730600732186

Blanpied, M. L., Marone, C., Lockner, D. A., Byerlee, J. D., & King, D. P. (1998). Quantitative measure of the variation in fault rheology due to fluid-rock interactions. *Journal of Geophysical Research*, *103*(B5), 9691–9712. https://doi.org/10.1029/98JB00162

Brantut, N., & Platt, J. D. (2017). Chapter 9: Dynamic weakening and the depth dependence of earthquake faulting Fault zone dynamic processes: Evolution of fault properties during seismic rupture. *Geophysical Monograph Series*, *227*, 171–194. https://doi.org/10.1002/9781119156895.ch9

Brantut, N., Schubnel, A., Corvisier, J., & Sarout, J. (2010). Thermochemical pressurization of faults during coseismic slip. *Journal of Geophysical Research*, *115*(B5), B05314. https://doi.org/10.1029/2009JB006533

Browne, P. R. L. (1978). Hydrothermal alteration in active geothermal fields. *Annual Review of Earth and Planetary Sciences*, *6*(1), 229–250. https://doi.org/10.1146/annurev.ea.06.050178.001305

Cappa, F., Scuderi, M. M., Collettini, C., Guglielmi, Y., & Avouac, J.-P. (2019). Stabilization of fault slip by fluid injection in the laboratory and in situ. *Science Advances*, *5*(3). eaau4065. https://doi.org/10.1126/sciadv.aau4065

Cathelineau, M., & Nieva, D. (1985). A chlorite solid solution geothermeter: The Los Azufres (Mexico) geothermal system. *Contributions to Mineralogy and Petrology*, *91*(3), 235–244. https://doi.org/10.1007/BF00413350

Cavarretta, G., Gianelli, G., & Puxeddu, M. (1982). Formation of authigenic minerals and their use as indicators of the physicochemical parameters of the fluid in the Larderello-Travale geothermal field. *Economic Geology*, *77*(5), 1071–1084. https://doi.org/10.2113/gsecongeo.77.5.1071

Chapman, T., Milan, L., & Vry, J. (2022). The role of metamorphic fluid in tectonic tremor along the Alpine Fault, New Zealand. *Geophysical Research Letters*, *49*, e2021GL096415. https://doi.org/10.1029/2021GL096415

Collettini, C., Niemeijer, A., Viti, C., & Marone, C. (2009). Fault zone fabric and fault weakness. *Nature*, *462*(7275), 907–910. https://doi.org/10.1038/nature08585

Davis, D. M., Suppe, J., & Dahlen, F. A. (1983). Mechanics of fold-and-thrust belts and accretionary wedges. *Journal of Geophysical Research*, *88*(B2), 1153–1172. https://doi.org/10.1029/JB088iB02p01153

de Barros, L., Daniel, G., Guglielmi, Y., Rivet, D., Caron, H., Payre, X., et al. (2016). Fault structure, stress, or pressure control of the seismicity in shale? Insights from a controlled experiment of fluid-induced fault reactivation. *Journal of Geophysical Research: Solid Earth*, *121*, 4506–4522. https://doi.org/10.1002/2015JB012633

den Hartog, S. A. M., & Spiers, C. J. (2013). Influence of subduction zone conditions and gouge composition on frictional slip stability of megathrust faults. *Tectonophysics*, *600*, 75–90. https://doi.org/10.1016/j.tecto.2012.11.006

den Hartog, S. A. M., & Spiers, C. J. (2014). A microphysical model for fault gouge friction applied to subduction megathrusts. *Journal of Geophysical Research: Solid Earth*, *119*, 1510–1529. https://doi.org/10.1002/2013JB010580

Dieterich, J. H. (1978). Time-dependent friction and the mechanics of stick-slip. *Pure and Applied Geophysics*, *116*(4–5), 790–806. https://doi.org/10.1007/BF00876539

Dieterich, J. H. (1979). Modeling of rock friction: 1. Experimental results and constitutive equations. *Journal of Geophysical Research*, *84*(B5), 2161–2168. https://doi.org/10.1029/JB084iB05p02161

Dieterich, J. H., & Kilgore, B. (1994). Direct observation of frictional contacts: New insights for state-dependent properties. *Pure and Applied Geophysics*, *143*(1–3), 283–302. https://doi.org/10.1007/BF00874332

Dieterich, J. H., & Kilgore, B. (1996). Implications of fault constitutive properties for earthquake prediction. *Proceedings of the National Academy of Sciences of the United States of America*, *93*(9), 3787–3794. https://doi.org/10.1073/pnas.93.9.3787

Elders, W. A., Hoagland, J. R., Mcdowell, S. D., & Cobo, J. (1979). Hydrothermal mineral zones in the geothermal reservoir of Cerro Prieto. *Geothermics*, *8*(3–4), 201–209. https://doi.org/10.1016/0375-6505(79)90042-7

Elsworth, D., Spiers, C. J., & Niemeijer, A. R. (2016). Understanding induced seismicity. *Science*, *354*(6318), 1380–1381. https://doi.org/10.1126/science.aal2584

Fagereng, Å., & Ikari, M. J. (2020). Low-temperature frictional characteristics of chlorite-epidote-amphibole assemblages: Implications for strength and seismic style of retrograde fault zones. *Journal of Geophysical Research: Solid Earth*, *125*, e2020JB019487. https://doi.org/10.1029/2020JB019487

Gebregzabher, Z. (1986). Hydrothermal alteration minerals in the Aluto Langano geothermal wells, Ethiopia. *Geothermics*, *15*(5–6), 735–740. https://doi.org/10.1016/0375-6505(86)90086-6

Giorgetti, C., Carpenter, B. M., & Collettini, C. (2015). Frictional behavior of talc-calcite mixtures. *Journal of Geophysical Research: Solid Earth*, *120*, 6614–6633. https://doi.org/10.1002/2015JB011970

Goebel, T., & Brodsky, E. (2018). The spatial footprint of injection wells in a global compilation of induced earthquake sequences. *Science*, *361*(6405), 899–904. https://doi.org/10.1126/science.aat5449

Grigoli, F., Cesca, S., Rinaldi, A. P., Manconi, A., López-Comino, J. A., Clinton, J. F., et al. (2018). The November 2017 Mw 5.5 Pohang earthquake: A possible case of induced seismicity in South Korea. *Science*, *360*(6392), 1003–1006. https://doi.org/10.1126/science.aat2010

Guglielmi, Y., Cappa, F., Avouac, J. F., Henry, P., & Elsworth, D. (2015). Seismicity triggered by fluid injection-induced aseismic slip. *Science*, *348*(6240), 1224–1226. https://doi.org/10.1126/science.aab0476

He, C., Wang, Z., & Yao, W. (2007). Frictional sliding of gabbro gouge under hydrothermal conditions. *Tectonophysics*, *445*(3–4), 353–362. https://doi.org/10.1016/j.tecto.2007.09.008

He, C., Yao, W., Wang, Z., & Zhou, Y. (2006). Strength and stability of frictional sliding of gabbro gouge at elevated temperatures. *Tectonophysics*, *427*(1–4), 217–229. https://doi.org/10.1016/j.tecto.2006.05.023

Hirose, T., & Bystricky, M. (2007). Extreme dynamic weakening of faults during dehydration by coseismic shear heating. *Geophysical Research Letters*, *34*, L14311. https://doi.org/10.1029/2007GL030049

Hong, T., & Marone, C. (2005). Effects of normal stress perturbations on the frictional properties of simulated faults. *Geochemistry, Geophysics, Geosystems*, *6*(3), Q03012. https://doi.org/10.1029/2004GC000821

Ikari, M. J., Carpenter, B. M., & Marone, C. (2016). A microphysical interpretation of rate- and state-dependent friction for fault gouge. *Geochemistry, Geophysics, Geosystems*, *17*(5), 1660–1677. https://doi.org/10.1002/2016GC006286

Ikari, M. J., Marone, C., & Saffer, D. M. (2011). On the relation between fault strength and frictional stability. *Geology*, *39*(1), 83–86. https://doi.org/10.1130/G31416.1

Ikari, M. J., Saffer, D. M., & Marone, C. (2009). Frictional and hydrologic properties of clay-rich fault gouge. *Journal of Geophysical Research*, *114*, B05409. https://doi.org/10.1029/2008JB006089

Ishibashi, T., Elsworth, D., Fang, Y., Riviere, J., Madara, B., Asanuma, H., et al. (2018). Friction-stability-permeability evolution of a fracture in granite. *Water Resources Research*, *54*, 9901–9918. https://doi.org/10.1029/2018WR022598

Kilgore, B. D., Blanpied, M. L., & Dieterich, J. H. (1993). Velocity dependent friction of granite over a wide range of conditions. *Geophysical Research Letters*, *20*(10), 903–906. https://doi.org/10.1029/93GL00368

Kim, K. H., Ree, J. H., Kim, Y. H., Kim, S., Kang, S. Y., & Seo, W. (2018). Assessing whether the 2017 Mw 5.4 Pohang earthquake in South Korea was an induced event. *Science*, *360*(6392), 1007–1009. https://doi.org/10.1126/science.aat6081

Kwiatek, G., Saarno, T., Ader, T., Bluemle, F., Bohnhoff, M., Chendorain, M., et al. (2019). Controlling fluid-induced seismicity during a 6.1-km-deep geothermal stimulation in Finland. *Science Advances*, *5*(5), eaav7224. https://doi.org/10.1126/sciadv.aav7224

Kwon, S., Xie, L., Park, S., Kim, K. I., Min, K. B., Kim, K. Y., et al. (2019). Characterization of 4.2-km-deep fractured granodiorite cores from Pohang geothermal reservoir, Korea. *Rock Mechanics and Rock Engineering*, *52*(3), 771–782. https://doi.org/10.1007/s00603-018-1639-2

Larochelle, S., Lapusta, N., Ampuero, J.-P., & Cappa, F. (2021). Constraining fault friction and stability with fluid-injection field experiments. *Geophysical Research Letters*, *48*, e2020GL091188. https://doi.org/10.1029/2020GL091188

Lee, K.-K., Yeo, I.-W., Lee, J.-Y., Kang, T.-S., Rhie, J., Sheen, D.-H., et al. (2019). *Summary report of the Korean Government commission on relations between the 2017 Pohang earthquake and EGS Project*. Geological Society of Korea and Korean Government Commission on the Cause of the Pohang Earthquake. Retrieved from https://www.gskorea.or.kr/custom/27/data/Summary_Report_on_Pohang_Earth-quake_March_20_2019.pdf

Logan, J. M., Dengo, C. A., Higgs, N. G., & Wang, Z. Z. (1992). Fabrics of experimental fault zones: Their development and relationship to mechanical behavior. In B. Evans, & T.-F. Wong (Eds.), *Fault mechanics and transport properties of rocks* (p. 3367). Academic Press. https://doi.org/10.1016/S0074-6142(08)62814-4

Marone, C. (1998). Laboratory-derived friction laws and their application to seismic faulting. *Annual Review of Earth and Planetary Sciences*, *26*(1), 643–696. https://doi.org/10.1146/annurev.earth.26.1.643

Martínez-Garzón, P., Kwiatek, G., Sone, H., Bohnhoff, M., Dresen, G., & Hartline, C. (2014). Spatiotemporal changes, faulting regimes, and source parameters of induced seismicity: A case study from the Geysers geothermal field. *Journal of Geophysical Research: Solid Earth*, *119*, 8378–8396. https://doi.org/10.1002/2014JB011385

Mitchell, E. K., Fialko, Y., & Brown, K. M. (2016). Velocity-weakening behavior of Westerly granite at temperature up to 600°C. *Journal of Geophysical Research: Solid Earth*, *121*, 6932–6946. https://doi.org/10.1002/2016JB013081

Moore, D. E., & Lockner, D. A. (2004). Crystallographic controls on the frictional behavior of dry and water saturated sheet structure minerals. *Journal of Geophysical Research*, *109*, B03401. https://doi.org/10.1029/2003JB002582

Niemeijer, A. R., & Collettini, C. (2014). Frictional properties of a low-angle normal fault under in situ conditions: Thermally-activated velocity weakening. *Pure and Applied Geophysics*, *171*(10), 2641–2664. https://doi.org/10.1007/s00024-013-0759-6

Niemeijer, A. R., & Spiers, C. J. (2007). A microphysical model for strong velocity weakening in phyllosilicate-bearing fault gouges. *Journal of Geophysical Research*, *112*, B10405. https://doi.org/10.1029/2007JB005008

Okamoto, A. S., Verberne, B. A., Niemeijer, A. R., Takahashi, M., Shimizu, I., Ueda, T., & Spiers, C. (2019). Frictional properties of simulated chlorite gouge at hydrothermal conditions: Implications for subduction megathrusts. *Journal of Geophysical Research: Solid Earth*, *124*, 4545–4565. https://doi.org/10.1029/2018JB017205

Olasolo, P., Juárez, M. C., Morales, M. P., Damico, S., & Liarte, I. A. (2016). Enhanced geothermal systems (EGS): A review. *Renewable and Sustainable Energy Reviews*, *56*, 133–144. https://doi.org/10.1016/j.rser.2015.11.031

Park, S., Kim, K., Xie, L., Yoo, H., Min, K., Kim, M., et al. (2020). Observations and analyses of the first two hydraulic stimulations in the Pohang geothermal development site, South Korea. *Geothermics*, *88*, 101905. https://doi.org/10.1016/j.geothermics.2020.101905

Passelègue, F. X., Brantut, N., & Mitchell, T. M. (2018). Fault reactivation by fluid injection: Controls from stress state and injection rate. *Geophysical Research Letters*, *45*, 12837–12846. https://doi.org/10.1029/2018GL080470

Reinen, L. A., & Weeks, J. D. (1993). Determination of rock friction constitutive parameters using an iterative least-squares inversion method. *Journal of Geophysical Research*, *98*(15), 15937–15950. https://doi.org/10.1029/93JB00780

Reyes, A. G. (1990). Petrology of Philippine geothermal systems and the application of alteration mineralogy to their assessment. *Journal of Volcanology and Geothermal Research*, *43*(1–4), 279–309. https://doi.org/10.1016/0377-0273(90)90057-M

Rice, J. R. (2006). Heating and weakening of faults during earthquake slip. *Journal of Geophysical Research*, *111*. B05311. https://doi.org/10.1029/2005JB004006

Ruina, A. (1983). Slip instability and state variable friction laws. *Journal of Geophysical Research*, *88*(B12), 10359–10370. https://doi.org/10.1029/JB088iB12p10359

Sáez, A., Lecampion, B., Bhattacharya, P., & Viesca, R. C. (2022). Three-dimensional fluid-driven stable frictional ruptures. *Journal of the Mechanics and Physics of Solids*, *160*, 104754. https://doi.org/10.1016/j.jmps.2021.104754

Saffer, D. M., & Marone, C. (2003). Comparison of smectite- and illite-rich gouge frictional properties: Application to the updip limit of the seismogenic zone along subduction megathrusts. *Earth and Planetary Science Letters*, *215*(1–2), 219–235. https://doi.org/10.1016/S0012-821X(03)00424-2

Sawai, M., Niemeijer, A. R., Plümper, O., Hirose, T., & Spiers, C. J. (2016). Nucleation of frictional instability caused by fluid pressurization in subducted blueschist. *Geophysical Research Letters*, *43*, 2543–2551. https://doi.org/10.1002/2015GL067569

Schiffman, P., & Fridleifsson, G. O. (1991). The smectite-chlorite transition in drillhole NJ-15, Nesjavellir geothermal field, Iceland: XRD, BSE and electron microprobe investigations. *Journal of Metamorphic Geology*, *9*(6), 679–696. https://doi.org/10.1111/j.1525-1314.1991.tb00558.x

Scholz, C. H. (1998). Earthquakes and friction laws. *Nature*, *391*(6662), 38–42. https://doi.org/10.1038/34097

Scholz, C. H. (2002). *The mechanics of earthquakes and faulting* (2nd ed., p. 91). Cambridge University Press.

Scuderi, M. M., & Collettini, C. (2018). Fluid injection and the mechanics of frictional stability of shale-bearing faults. *Journal of Geophysical Research: Solid Earth*, *123*, 8364–8384. https://doi.org/10.1029/2018JB016084

Scuderi, M. M., Collettini, C., & Marone, C. (2017). Frictional stability and earthquake triggering during fluid pressure stimulation of an experimental fault. *Earth and Planetary Science Letters*, *477*, 84–96. https://doi.org/10.1016/j.epsl.2017.08.009

Seki, Y., Liou, J. G., Gillemette, R., Sakai, H., Oki, Y., Hirano, T., et al. (1983). *Investigation of geothermal systems in Japan I. Onikobe geothermal area*. Hydroscience and Geotechnology Laboratory, Saitama University.

Steiner, A. (1968). Clay minerals in hydrothermally altered rocks at Wairakei, New Zealand. *Clays and Clay Minerals*, *16*(3), 193–213. https://doi.org/10.1346/CCMN.1968.0160302

Tembe, S., Lockner, D. A., & Wong, T.-F. (2010). Effect of clay content and mineralogy on frictional sliding behavior of simulated gouges: Binary and ternary mixtures of quartz, illite, and montmorillonite. *Journal of Geophysical Research*, *115*, B03416. https://doi.org/10.1029/2009JB006383

Walsh, F. R., & Zoback, M. D. (2015). Oklahoma's recent earthquakes and saltwater disposal. *Science Advances*, *1*(5), e1500195. https://doi.org/10.1126/sciadv.1500195

Wibberley, C. A., & Shimamoto, T. (2005). Earthquake slip weakening and asperities explained by thermal pressurization. *Nature*, *436*(7051), 689–692. https://doi.org/10.1038/nature03901

Wong, T.-F., & Baud, P. (2012). The brittle-ductile transition in porous rock: A review. *Journal of Structural Geology*, *44*, 25–53. https://doi.org/10.1016/j.jsg.2012.07.010

Yasuhara, H., & Elsworth, D. (2004). Evolution of permeability in a natural fracture: Significant role of pressure solution. *Journal of Geophysical Research*, *109*, B03204. https://doi.org/10.1029/2003JB002663